Growth mechanism and internal structure of vertically aligned single-walled carbon nanotubes

Erik Einarsson[1], Masayuki Kadowaki[1], Kazuaki Ogura[1], Jun Ookawa[1], Rong Xiang[1],

Zhengyi Zhang[1], Takahisa Yamamoto[2], Yuichi Ikuhara[3], Shigeo Maruyama[1*]

[1]*Dept. of Mechanical Engineering, The Univeristy of Tokyo*

[2]*Dept. of Advanced Materials Science, The Univeristy of Tokyo*

[3]*Institute of Engineering Innovation, The University of Tokyo*

Abstract

In this study we used an *in situ* optical absorbance technique to monitored the growth of vertically aligned single-walled carbon nanotubes (VA-SWNTs) at various temperatures and pressures. This yielded a profile of the VA-SWNT thickness vs growth time, which was analyzed using a growth model. The dependence on growth pressure and temperature of two characteristic parameters, the initial growth rate and reaction time constant, were investigated. We found that the ideal pressure for VA-SWNT synthesis changes systematically with the growth temperature, shifting toward higher pressure as the growth temperature increases. We also show the initial growth rate increases linearly with pressure up to approximately $2\,\mathrm{kPa}$, and decreasing at still higher pressures. This linear behavior indicates the growth reaction is first-order in this pressure range. We also studied the internal structure of the VA-SWNT array by transmission electron microscope observation at different depths into the VA-SWNT array.

Keywords: carbon nanotube, SWNT, alcohol CVD, growth mechanism, TEM

* Electronic address: maruyama@photon.t.u-tokyo.ac.jp

I. INTRODUCTION

Single-walled carbon nanotubes (SWNTs) are known for their unique physical properties, which arise from their one-dimensional structure [1–3]. Some of these properties, such as near-ballistic transport [4], anisotropic optical absorption [5–8] and high thermal conductivity [9–11] make SWNTs particularly well-suited for various advanced applications. In order to exploit these properties, however, it is necessary to be able to control the location, size, and morphology of the SWNTs. The last few years have seen several advancements in these areas, particularly regarding the synthesis of vertically aligned (VA-)SWNTs [12–19]. Synthesis of SWNTs, however, is a process which depends on many parameters (temperature, pressure, flow rate, etc.), and understanding the many relations in this multi-parameter space is quite complicated. Here we report some advancements in this area, where the effects of growth temperature and pressure on VA-SWNT growth, particularly the initial growth rate, were investigated. We also discuss the internal structure of these aligned SWNT films, directly observed in their aligned state by transmission electron microscopy.

II. EXPERIMENTAL PROCEDURES

The VA-SWNTs investigated in this study were synthesized by the alcohol catalytic chemical vapor deposition (ACCVD) method [12, 20]. This method produces high-purity SWNTs with very little formation of amorphous carbon or other byproducts. Synthesis is carried out inside a conventional CVD chamber, with temperatures between 600 and 800 °C, and at an ambient pressure of approximately 1.4 kPa (10 Torr). The metal catalyst particles with which the alcohol react are prepared by a dip-coat method [21], where the growth substrate (usually quartz) is immersed into two different solution of dissolved metal salts, then slowly withdrawn at a speed of $4\,\mathrm{cm\,s^{-1}}$. The first solution contains molybdenum acetate, $(CH_3COO)_2Mo$, dissolved in ethanol (Mo content 0.01 wt%). After withdrawing the substrate, it is baked in air at 400 °C for 5 minutes, which removes the acetate and oxidizes the deposited metals. This prevents thermal migration of the metal particles at elevated temperatures, which often results in agglomeration and formation of larger particles that are not conducive to SWNT growth. After baking the dip-coated substrate, these steps are repeated using a solution of cobalt acetate, $(CH_3COO)_2Co\text{-}4H_2O$, also dissolved in ethanol
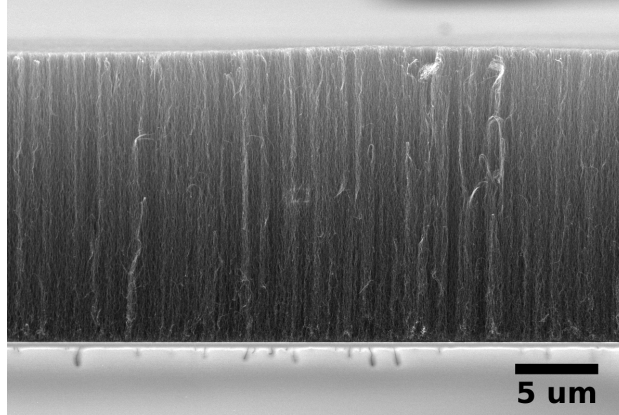
2

FIG. 1: SEM image of a VA-SWNT film synthesized from alcohol. The film thickness is approx. $16.5\,\mu$m.

at the same concentration (0.01 wt% Co). Using this bimetal approach, the Mo forms an oxide layer that is believed to stabilize the pure Co metal particles [22], where the Co is the catalyst driving SWNT growth.

VA-SWNTs are synthesized by placing the dip-coated substrate in the CVD chamber, then heating up to the growth temperature (typically 800 °C) under 40 kPa of flowing Ar/H$_2$ (3% H$_2$, Ar balance, flow rate of 300 sccm). Once reaching the growth temperature, the Ar/H$_2$ flow is stopped, and 99.5% dehydrated ethanol is introduced into the chamber at a flow rate of 300 to 500 sccm and a pressure of 1-2 kPa (7-15 Torr). VA-SWNTs synthesized by this method are shown in Fig. 1. While inside the CVD chamber, the optical absorbance of the VA-SWNT film can be measured throughout the growth process. Based on the correlation between VA-SWNT film thickness and absorbance [23, 24], this *in situ* absorption measurement allows one to observe the growth process as well as control the final film thickness by stopping the alcohol flow at the appropriate point during growth.

III. RESULTS & DISCUSSION

A. Internal structure of VA-SWNTs

Electron microscopy techniques are extremely valuable in SWNT characterization, providing information on the overall morphology by scanning electron microscopy (SEM), and information at the scale of individual SWNTs by transmission electron microscopy (TEM).

Unfortunately, sample preparation for TEM observation usually involves dispersion of the SWNTs and placing some of this dispersion onto a TEM grid. This obviously destroys the aligned morphology of as-grown SWNT arrays, making it impossible to observe them in their aligned state. Recently, however, our group has succeeded in imaging SWNTs in their aligned state [25] by transferring the as-grown films onto a TEM grid using a hot-water assisted method [26] that allows removal and transfer of the VA-SWNTs while preserving the SWNT alignment. Using the same preparation technique, we have again observed VA-SWNTs by TEM, but this time scanned the focal plane through the sample. This approach yields cross-sectional images at different depths into the VA-SWNT film.

The VA-SWNT observed had thickness of $4\,\mu$m, similar to that shown in Fig. 2a. The VA-SWNTs were transferred onto a TEM grid by the hot-water method mentioned above [26], and imaged from the top of the film (plan view), such that the perspective is along the SWNT alignment direction. Cross-sectional images of the film were obtained at different depths into the VA-SWNT array by changing the focal plane while keeping the sample position fixed. Figures 2b - 2d show three cross-sectional images of the VA-SWNT film obtained at 0, 600, and 900 nm into the film, which are indicated by the dashed lines in Fig. 2a. The distance was measured from the focal plane of Fig. 2b (0 nm), taken at the top of the film. There is little change in the images over this distance, which is expected due to the alignment of the SWNTs. The clearest difference is the bundle cross-section in the lower-center of the image, which goes from under-focused to in-focus, then to over-focused. Other regions are very obscure because the film is a bit too thick for clear imaging of this kind. One thing that is clear, however, is that the SWNT bundles are very small, in agreement with previous TEM observations [25]. The bundle near the center of the images, which is typical, contains approximately eight SWNTs. This small bundle size is believed to preserve the 1D optical properties of the SWNTs [25, 27], which in large bundles would be altered by tube-tube interactions to the point that the electrical properties of the SWNTs more closely resemble those of bulk graphite.

In addition to SEM and TEM, resonance Raman scattering is a very simple, yet powerful tool for characterization of SWNTs. A typical Raman spectrum from VA-SWNTs grown from alcohol is shown in Fig. 3 (thick line). The sharp, strong G-band peak at $1592\,\mathrm{cm}^{-1}$ relative to the weak D-band peak near $1350\,\mathrm{cm}^{-1}$ reflects the high purity of the SWNTs [28]. The radial breathing mode (RBM) peaks found between 100 and $300\,\mathrm{cm}^{-1}$ are shown in the
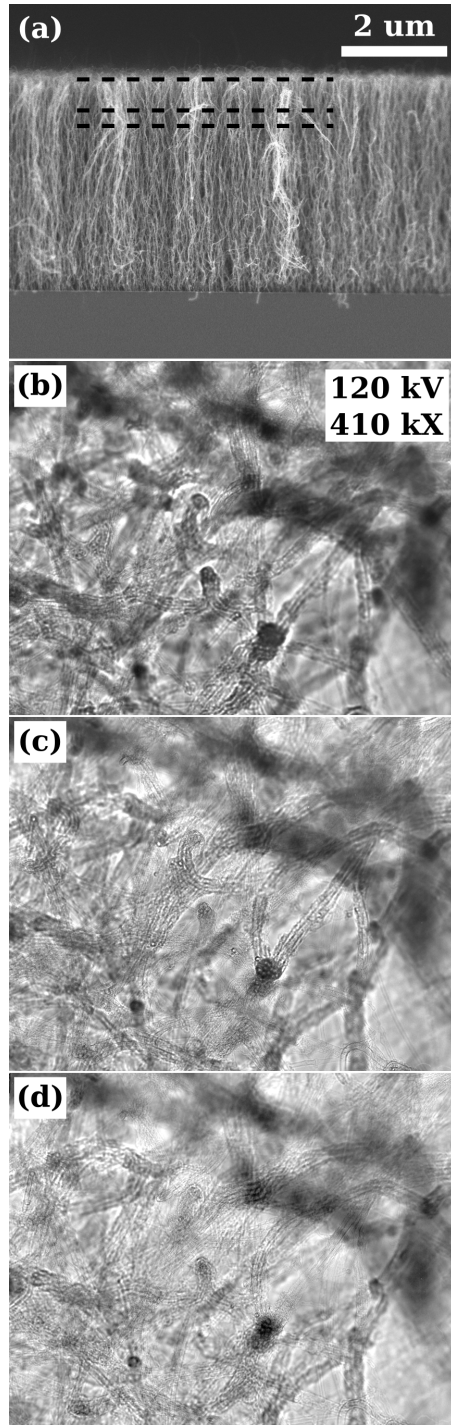
FIG. 2: (a) SEM image of a 4-μm-thick VA-SWNT array. (b) Cross-sectional TEM image of the top of the array, (c) another TEM image at the same location, but with the focal plane shifted 600 nm down into the array, and (d) another image at a depth of 900 nm. Image depths in (b)-(d) are marked by dashed lines in (a).
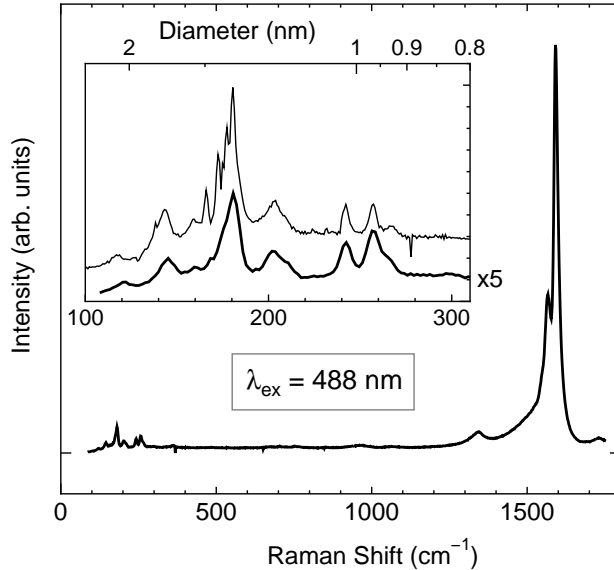
FIG. 3: Typical resonance Raman spectrum from VA-SWNTs (thick line) using a standard $1200\,\text{mm}^{-1}$ grating. The RBM peaks are shown in the inset, and compared to another spectrum obtained with a higher resolution $2400\,\text{mm}^{-1}$ grating. The dominant peak at $180\,\text{cm}^{-1}$ is found to split into separate, closely spaced peaks.

inset. The diameter scale on the upper axis was determined from the relationship between the RBM frequency and the SWNT diameter [28], $d_t = 248/\omega_{RBM}$ $[\text{cm}^{-1}]$. The dominant peak near $180\,\text{cm}^{-1}$ arises from excitation by perpendicularly-polarized light, which excites non-vertical ($\Delta\mu = \pm 1$) transitions [29]. This is a strong indicator of vertical alignment of the SWNTs when the Raman spectra are measured from the top of the VA-SWNT film.

The spectrum shown by the thick line was obtained with a $1200\,\text{mm}^{-1}$ grating, which provides a balance of good resolution and enough spectral range to observe the RBM, D-band, and G-band peaks in the same spectrum. The thin line in the inset is a high-resolution spectrum obtained only for the RBM region using a $2400\,\text{mm}^{-1}$ grating. This high-resolution spectrum reveals the characteristic $180\,\text{cm}^{-1}$ peak actually consists of several sharp, closely spaced peaks. As with the peak at $180\,\text{cm}^{-1}$, these peaks are believed to arise from Raman scattering of perpendicularly-polarized light. Since the presence of neighboring SWNTs can significantly affect the Raman modes [30] may be due to the thin bundles such as those in Fig. 2 and reported in [25]. Additional investigation is necessary, however, to clarify the origin of these peaks.

B. Analysis of growth parameters

As mentioned in the previous section, the optical absorbance of a VA-SWNT array is proportional to the thickness of the array [23], thus one can observe the growth in near real-time by measuring the optical absorbance during the CVD process. Such an *in situ* method has been used to study VA-SWNT growth [24], from which a model describing the growth process was proposed. According to this model, VA-SWNT growth can be described by two parameters, the initial growth rate γ_0 [μm s^{-1}], and a catalyst activity time constant, τ [s]. The expression for the overall film thickness, L [μm] is

$$L(t) = \gamma_0 \tau \left(1 - e^{-t/\tau} \right). \tag{1}$$

From this equation, one can see that the maximum (final) film thickness at $L(t \to \infty)$ is $\gamma_0 \tau$, appropriately determined by the two growth parameters.

Figure 4a shows the effect of ethanol pressure on the final thickness, $\gamma_0 \tau$, of VA-SWNTs produced at different temperatures. These data show that the pressure at which maximum growth occurs is dependent on the growth temperature, and this 'ideal' pressure increases with higher temperature. This trend is shown in Fig. 4b, where the pressure at which maximum VA-SWNT film thickness was achieved is plotted for each growth temperature. Although there are few data, the trend in this temperature range is apparent. These results are further decomposed in Fig. 5a and Fig. 5b, which show the effect of pressure on each of the growth parameters, independently. The values of γ_0 and τ were obtained by iterative fitting to the experimental data (not shown) using eqn. (1). In Fig. 5a we see the pressure dependence of γ_0, which increases in a linear fashion, regardless of the growth temperature. This increase continues until approximately $2\,\text{kPa}$, above which γ_0 begins to decrease. Since there are few data in this higher pressure range, it is unclear whether γ_0 will decrease back down toward zero as the pressure continues to climb, or if it will plateau at some value. Below $2\,\text{kPa}$, however, the linear correlation between the initial growth rate and the ethanol pressure indicates the growth reaction is a first-order reaction. This is significant because it shows the growth reaction is simple dissociation of ethanol at the catalyst particle, rather than a complex process involving intermediate steps and interference by reaction byproducts. Such knowledge of the type of reaction is important in understanding the fundamental underlying synthesis mechanism.
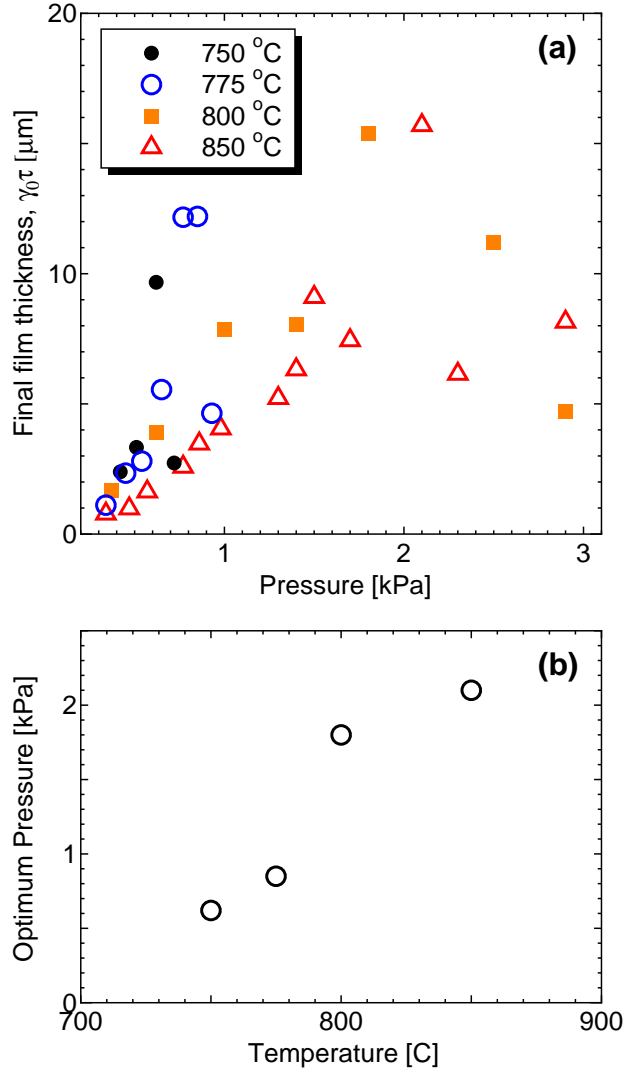
FIG. 4: (a) overall growth vs. ethanol pressure for different growth temperatures, and (b) pressure at which maximum growth occurs for a given growth temperature

Figure 5b shows the dependence of the time constant, τ, on the ethanol pressure. Unlike γ_0, there is no clear pressure-temperature dependence. It seems τ is largely independent of pressure, with the exception of an apparent sharp increase in the time constant at lower pressures. If the catalyst activity diminishes at a rate proportional to the growth rate – as postulated in the growth model [24] – then τ should be rather constant, decreasing faster when γ_0 is larger and more slowly when γ_0 is small. This could explain the insensitivity of τ to pressure for the majority of the pressure range shown in Fig. 5b. At low pressures, however, where the growth rate is very slow, the process by which the catalyst activity diminishes may be different, which is responsible for the increase in τ. Of course this is very
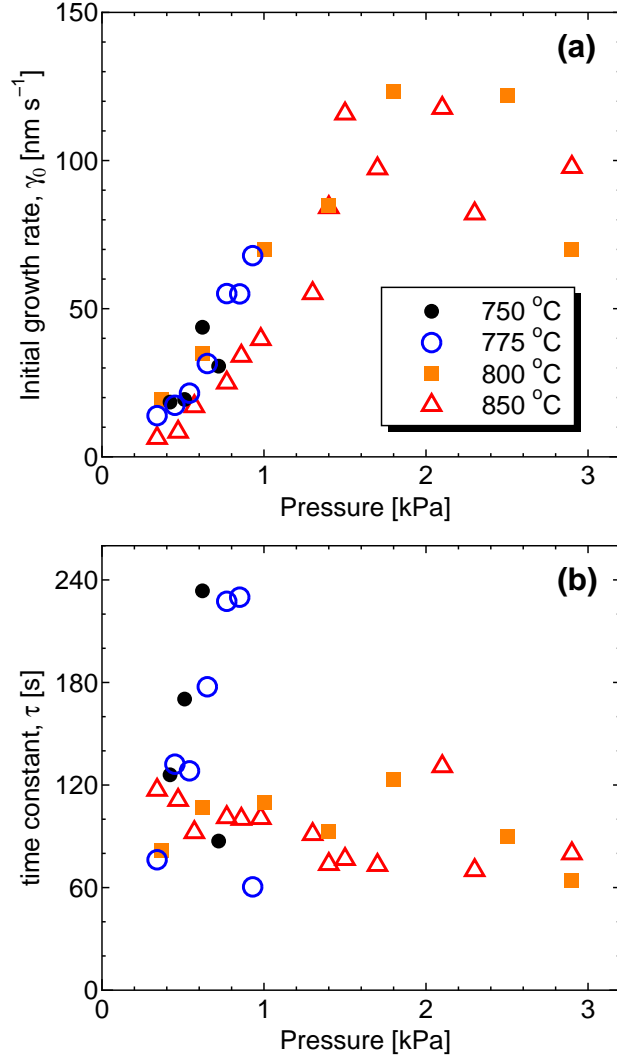
8

FIG. 5: Change in (a) initial growth rate γ_0 and (b) time constant τ as a function of ethanol pressure.

speculative at this point, and further investigation is necessary to clarify the mechanism responsible for the diminishing catalyst activity.

IV. SUMMARY

We have presented the latest results of our investigation of the synthesis of VA-SWNTs. An *in situ* optical absorption method was used to investigate the role of temperature and pressure on the initial growth rate of the VA-SWNT film and the catalyst activity time constant. These results show the initial growth rate increases linearly with pressure, and

then decreases above approximately $2\,\mathrm{kPa}$. This indicates that below $2\,\mathrm{kPa}$ – where VA-SWNT synthesis usually occurs – the growth reaction is first-order. The catalyst activity time constant, on the other hand, was largely unaffected by temperature and pressure. A better understanding of the roles of the many synthesis parameters is critical not only to improving SWNT synthesis, but also to determining the underlying reaction mechanism.

We also show that high-resolution Raman spectroscopy reveals previously overlooked structure in the RBM peaks, particularly around $180\,\mathrm{cm}^{-1}$. The origin of these tightly-grouped peaks is still unclear, but is thought to be related to the small-bundle structure of the arrays observed by TEM.

Acknowledgments

---

[1] R. Saito, G. Dresselhaus, and M. S. Dresselhaus, *Physical Properties of Carbon Nanotubes* (Imperial College Press, London, 1998).

[2] M. S. Dresselhaus, G. Dresselhaus, and P. Avouris, *Carbon Nanotubes: Synthesis, Structure, Properties, and Applications*, vol. 80 (Springer, Berlin, 2001).

[3] Z. Yao, C. Dekker, and P. Avouris, Top. Appl. Phys. **80**, 147 (2001).

[4] N. Mingo and D. Broido, Phys. Rev. Lett. **95**, 096105 (2005).

[5] J. Hwang, H. H. Gommans, A. Ugawa, H. Tashiro, R. Haggenmueller, K. I. Winey, J. E. Fischer, D. B. Tanner, and A. G. Rinzler, Phys. Rev. B **62**, R13310 (2000).

[6] M. Ichida, S. Mizuno, H. Kataura, Y. Achiba, and A. Nakamura, Appl. Phys. A **78**, 1117 (2004).

[7] M. F. Islam, D. E. Milkia, C. L. Kane, A. G. Yodh, and J. M. Kikkawa, Phys. Rev. Lett. **93**, 037404 (2004).

[8] Y. Murakami, E. Einarsson, T. Edamura, and S. Maruyama, Phys. Rev. Lett. **94**, 087402 (2005).

[9] S. Maruyama, Physica B **323**, 193 (2002).

[10] C. Yu, L. Shi, Z. Yao, D. Li, and A. Majumdar, Nano Lett. **5**, 1842 (2005).

[11] E. Pop, D. Mann, Q. Wang, K. Goodson, and H. Dai, Nano Lett. **6**, 96 (2006).

[12] Y. Murakami, S. Chiashi, Y. Miyauchi, M. Hu, M. Ogura, T. Okubo, and S. Maruyama, Chem. Phys. Lett. **385**, 298 (2004).

[13] K. Hata, D. N. Futaba, K. Mizuno, T. Namai, M. Yumura, and S. Iijima, Science **306**, 1362 (2004).

[14] G. Zhong, T. Iwasaki, K. Honda, Y. Furukawa, I. Ohdomari, and H. Kawarada, Chem. Vap. Dep. **11**, 127 (2005).

[15] G. Zhang, D. Mann, L. Zhang, A. Javey, Y. Li, E. Yenilmez, Q. Wang, J. P. McVittie, Y. Nishi, J. Gibbons, et al., PNAS **102**, 16141 (2005).

[16] G. Eres, A. A. Kinkhabwala, H. Cui, D. B. Geohegan, A. A. Puretzky, and D. H. Lowndes, J. Phys. Chem. B **109**, 16684 (2005).

[17] Y.-Q. Xu, E. Flor, M. J. Kim, H. Behrang, H. Schmidt, R. E. Smalley, and R. H. Hauge, J. Am. Chem. Soc. **128**, 6560 (2006).

[18] L. Zhang, Y. Tan, and D. E. Resasco, Chem. Phys. Lett. **422**, 198 (2006).

[19] S. Noda, H. Sugime, T. Osawa, T. Yoshiko, S. Chiashi, Y. Murakami, and S. Maruyama, Carbon **44**, 1414 (2006).

[20] S. Maruyama, R. Kojima, Y. Miyauchi, S. Chiashi, and M. Kohno, Chem. Phys. Lett. **360**, 229 (2002).

[21] Y. Murakami, Y. Miyauchi, S. Chiashi, and S. Maruyama, Chem. Phys. Lett. **377**, 49 (2003).

[22] M. Hu, Y. Murakami, M. Ogura, S. Maruyama, and T. Okubo, J. Catal. **225**, 230 (2004).

[23] S. Maruyama, E. Einarsson, Y. Murakami, and T. Edamura, Chem. Phys. Lett. **403**, 320 (2005).

[24] E. Einarsson, Y. Murakami, M. Kadowaki, and S. Maruyama, submitted to Carbon.

[25] E. Einarsson, H. Shiozawa, C. Kramberger, M. H. Rümmeli, A. Grüneis, T. Pichler, and S. Maruyama, submitted to J. Phys. Chem. B.

[26] Y. Murakami and S. Maruyama, Chem. Phys. Lett. **422**, 575 (2006).

[27] T. Pichler, et al., unpublished.

[28] A. Jorio, M. Pimenta, A. S. Filho, R. Saito, G. Dresselhaus, and M. Dresselhaus, New J. Phys. **5**, 139 (2003).

[29] Y. Murakami, S. Chiashi, E. Einarsson, and S. Maruyama, Phys. Rev. B **71**, 085403 (2005).

[30] A. Jorio, A. S. Filho, V. Brar, A. Swan, M. Ünlü, B. Goldberg, A. Righi, J. Hafner, C. Lieber, R. Saito, et al., Phys. Rev. B **65**, 121402(R) (2002).